In-situ study of ammonium bromide formation for optimizing boron nitride ALD from BBr_3 and NH_3

Arnoud J. Onnink, R. Oguzhan Apaydin, Jurriaan Schmitz and Alexey Y. Kovalgin

MESA+ Institute for Nanotechnology, University of Twente, the Netherlands. E-mail: a.j.onnink@utwente.nl

Boron nitride (BN) has received much attention for a wide range of applications, including in electronics, photonics, and power devices [1]. Among the variety of techniques to deposit thin films of BN, atomic layer deposition (ALD) is an industrially relevant approach due to enabling precise thickness control and excellent conformality [1].

This work studies the deposition of BN from boron tribromide (BBr_3) and ammonia (NH_3) by *in-situ* real-time monitoring of the reactive gases and reaction byproducts, using Fourier Transform infrared (FTIR) spectroscopy and spectroscopic ellipsometry (SE) as schematically shown in figure 1a. Depending on the chosen conditions, the deposition of BN varies between ALD and pulsed chemical vapor deposition (CVD). Figures 1b-c show a layer of particles deposited on a cold (293 K) substrate near the exhaust, identified as ammonium bromide (NH_4Br) by the FTIR reflectance spectrum. Such salt is a known byproduct in CVD from NH_3 and halide precursor [2], forming from NH_3 and the gaseous hydrogen halide byproduct (here, HBr) and spreading through the reactor by sublimation, dissociation [3] to HBr + NH_3, and redeposition.

To optimize an ALD recipe, the precursor-pulse and purge durations are typically increased until the growth per cycle (GPC) saturates. This work explores a new method to optimize BN ALD based on *in-situ* monitoring by FTIR and SE of the precursors and reaction byproducts. The idea is as follows. First, FTIR monitoring detects precursor mixing (PM) in real-time and thus assists in minimizing that effect. Second, the quantity of NH_4Br formed per cycle is expected to indicate a degree of PM. Figure 2a demonstrates the concept, which is understood by the model given below.

In absence of PM, only the fraction of HBr that is produced in the NH_3 pulse forms NH_4Br. BN ALD will thus form less NH_4Br than CVD; the amount depends on the mechanism. Based on the known mechanism of thermal ALD of aluminum nitride and the recently proposed similar pathway for gallium nitride from NH_3 and trimethylgallium [4], we hypothesize that ALD of BN involves formation of a -BBr:NH_3 'surface adduct' complex, subsequently converted to B–NH_2–B links. This reaction produces 1 mol of HBr per mol of BN in the NH_3 pulse, and so 1 mol of NH_4Br. The remaining hydrogen atoms of the –NH_2-termination are released in the BBr_3 pulse (i.e., –NH_2 + BBr_3 → 2 HBr + –N-B-Br) in absence of NH_3. Alternative ALD mechanisms may yield higher NH_4Br production, but not exceeding 3 mol per mol BN. With PM, at least 3 mol NH_4Br is made per mol BN, or more if BBr_3 reacts with gases such as H_2O to form additional HBr. Therefore, the monitoring of NH_4Br production can yield information on the mode and mechanism of pulsed BN deposition.

The conditions that minimize PM in a BN deposition can be predicted by a model that describes the rise (pulse), decay (purge), and fall (reaction) in the precursor partial pressures. Figure 2b shows such a model, that also incorporates HBr and the growth of NH_4Br through parameters determined from combined *in-situ* SE and FTIR data (e.g., fig. 2a). Process 2 approaches the NH_4Br GPC of ALD, whereas process 1 is in CVD mode. An extensive purge is required to prevent PM fully; the duration may be shortened by minimizing the pulse dose and reactor volume, and maximizing the pump speed.

The monitoring of experimental trends in the NH_4Br production can further clarify the BN growth mechanism. If BN growth occurs via reversible formation of -BBr:NH_3 surface adducts, then the equilibrium concentration of these adducts should increase with the partial pressure of NH_3 (pNH_3), enhancing the formation of B–NH_2–B links. Our separately submitted results [5] indeed show the expected dependence of the BN GPC on pNH_3, which is rather atypical for ALD. In support of this result, figure 3a demonstrates that the NH_4Br production per cycle is also pressure-dependent. A lower pressure results in increased NH_4Br production, presumably because the BN growth mechanism transitions from adduct-dominated to a different regime in which more than 1 unit of HBr is produced per unit of BN during the NH_3 pulse.

Figure 3 displays the surprising observation that NH_4Br deposition on the monitor wafer can be delayed to over an hour after the end of BN deposition. Based on the absence of HBr (figure 3a, inset) at the exhaust during the delay, we suggest that free HBr has a short lifetime when chamber surfaces have a high density of adsorbed NH_3. Then, all NH_4Br produced after the first cycle initially deposits on cold surfaces near the deposition compartment only. Any decomposition to HBr + NH_3 is quickly followed by redeposition, until the density of NH_3 is sufficiently reduced to allow migration (figure 3b).

In summary, our presentation will discuss the optimization of pulsed BN deposition from NH_3 and BBr_3 towards ALD, assessing the effect of precursor mixing by detailed *in-situ* monitoring of the gas phase and the production of NH_4Br.

[1] M. Weber et al. *CrystEngComm* 19(41) (2017) 6089-6094 and references therein.
[2] B.J. Choi, D.W. Park, D.R. Kim. *J. Mater. Sci. Lett.* 14(6) (1995) 452–454.
[3] R.S. Zhu, J.H. Wang, M.C. Lin. *J. Phys. Chem. C* 111(37) (2007), 13831-13838.
[4] S. Banerjee et al. *J. Phys. Chem. C* 122(51) (2018), 29567–29576.
[5] R.O. Apaydin, A.A.I. Aarnink, M. P. de Jong, D.J. Gravesteijn, A.Y. Kovalgin. Submitted to EuroCVD 2019.

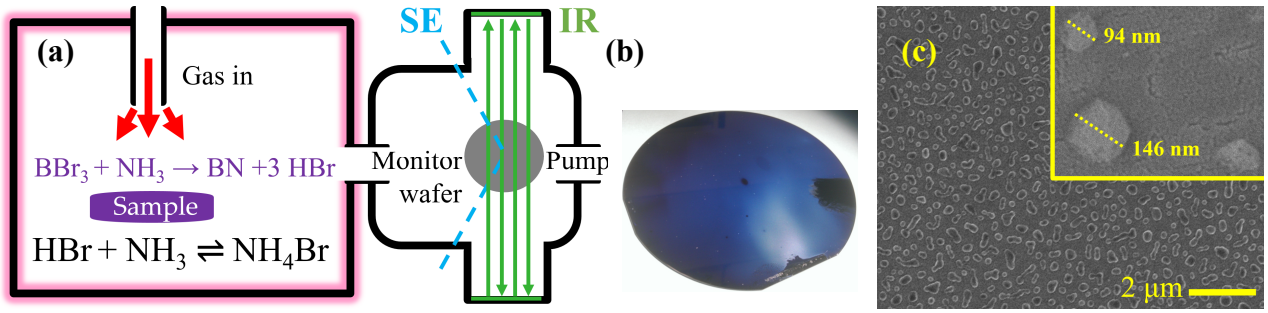

Figure 1. (a) Schematic overview of the studied reactions and the reactor (not to scale), comprising a BN deposition compartment (345 K walls) and an attachment (293 K) with *in-situ* spectroscopic ellipsometer (SE) and infrared (IR) spectrometer. The IR beam reflects between aluminum mirrors to a total path length of 26 m. **(b)** Photo of monitor wafer with a NH_4Br film (partially cleaned for contrast). **(c)** Scanning electron micrographs of NH_4Br nanoparticles on (b).

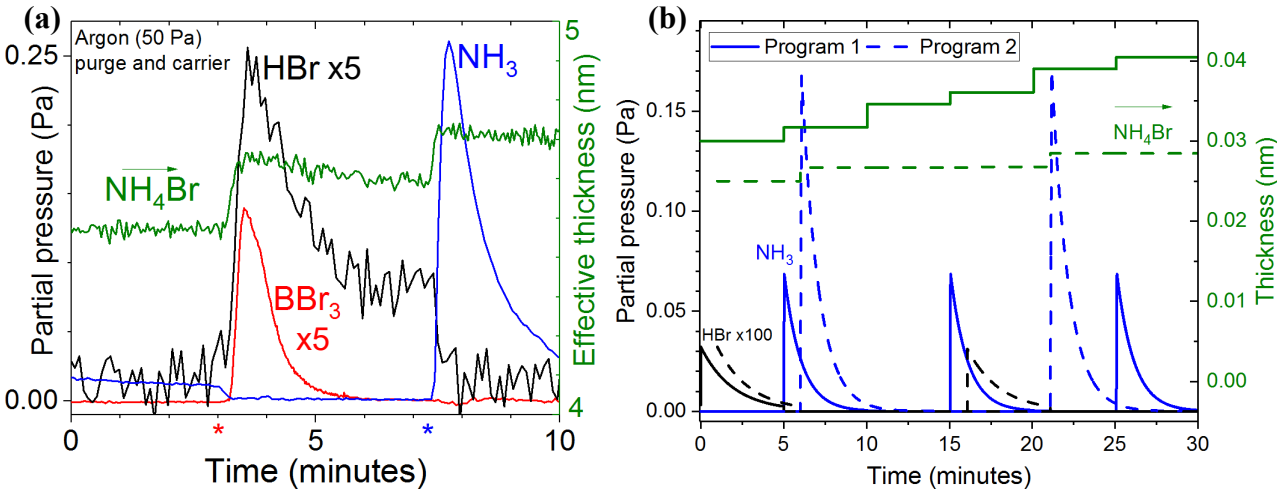

Figure 2. (a) *In-situ* monitoring of gases (FTIR) and the monitor wafer (SE) near the exhaust during pulsed BN deposition. A pulse of BBr_3 (30 s) is started at $t = 3$ min with 0.01 Pa of NH_3 still present, leading to production of NH_4Br and HBr and rapid decay of pNH_3. A subsequent pulse of NH_3 (5 s) in the presence of HBr similarly leads to NH_4Br production. (Partial pressures were calculated from the integrated absorbance of peaks in FTIR spectra. The effective NH_4Br thickness is calculated as layer thickness×(1-void fraction) from fits to SE data.) **(b)** Simulated pulsed depositions with different pulse and purge durations. Program 1 leads to significant PM and high NH_4Br GPC. Program 2 approaches ALD, as most HBr produced in the BBr_3 pulse is pumped off rather than reacting with NH_3 to form NH_4Br. The model calculates the NH_4Br production assuming instantaneous reactions (not treating transport or kinetics): experimentally, when either HBr or NH_3 is present in excess, the other species is not detected by *in-situ* FTIR, consistent with full conversion to NH_4Br. Durations in seconds (BBr_3 pulse, Ar purge, NH_3 pulse, Ar purge), program 1: 0.1-300-2-300, program 2: 0.1-300-5-600.

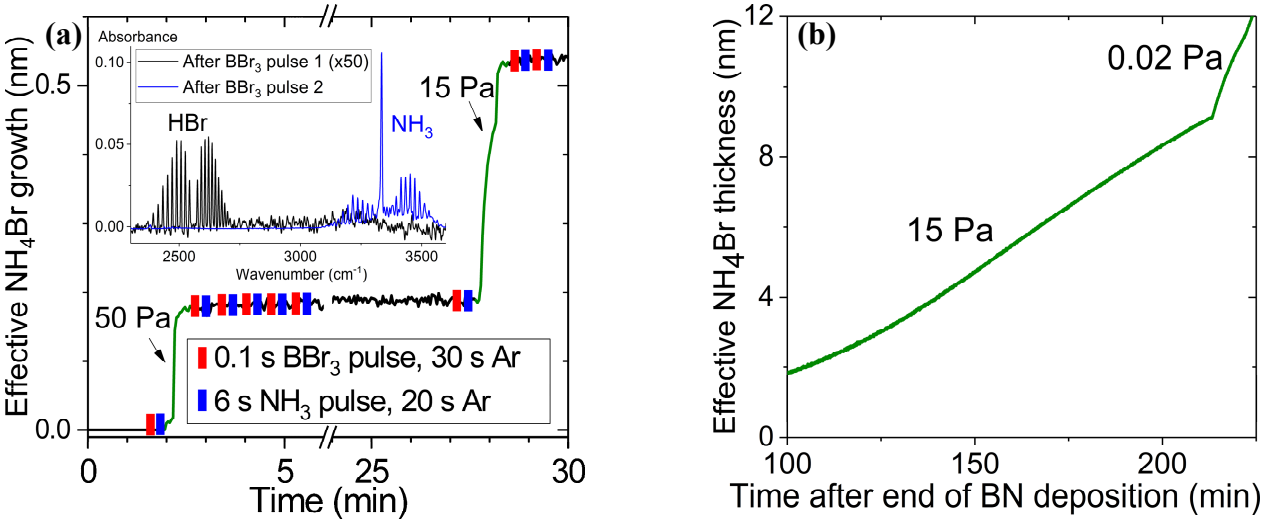

Figure 3. (a) During pulsed BN deposition with purge duration < 1 minute, NH_4Br only deposits on the monitor wafer in the first pulse-purge cycle. In subsequent cycles and until a 10 minute purge, *in-situ* FTIR monitoring (inset) detects NH_3 but not HBr. This figure also shows that the NH_4Br GPC on the monitor wafer increases as pressure is decreased. **(b)** After the BN deposition started in (a) is completed, NH_4Br migrates from the deposition chamber to the monitor wafer.

Kinetic analysis on TiAlN-CVD to construct reaction model

Jun Yamaguchi[1], Tomoko Hirabaru[1], Hayato Kubo[2], Momoko Deura[1], Takeshi Momose[1], Takahito Tanibuchi[2], and Yukihiro Shimogaki[1]

1 Department of Materials Engineering, The University of Tokyo, Japan
(yamaguchi@dpe.mm.t.u-tokyo.ac.jp)
2 Cutting Tool R&D Division, Kyocera Corporation, Japan

1. Introduction

Cutting tools are consist of cemented carbides, typically tungsten carbide (WC), covered with a hard ceramic film. Combination of high toughness of cemented carbides and high wear resistance of ceramic films enable excellent cutting performance and a long lifetime. Cubic-TiAlN is a next-generation coating material rather than various candidates including TiCN and Al_2O_3 because of high hardness and chemical stability. As for the TiAlN films grown by PVD, both mechanical and chemical properties improved with the higher Al composition but degraded above 67% due to formation of softer hexagonal-TiAlN [1], which is consistent with the phase diagram. In the meantime, Endler *et al*. have succeeded in synthesizing metastable cubic-TiAlN film with the Al composition of 90% by CVD [2]. We have investigated the process conditions thereby achieved the cubic-TiAlN with the Al composition of 94%, whose mechanical and chemical properties are satisfactory for the industrial application. Remaining issues are to rigorously control the properties of cubic-TiAlN films grown by CVD and design the mass-productive reactor without the conventional approaches of trial-and-error optimization. Accordingly, computational simulation is mandatory, which is capable of predicting the film thickness profile within a reactor. However, clear and valid understanding on the reaction mechanism is still inadequate. Therefore, we still have to extract kinetic information from experiments. In this study, we performed kinetic analyses to clarify the reaction mechanism of cubic-TiAlN-CVD by identifing the main reaction path and deposition species.

2. Experiments

We deposited TiAlN films at 800 °C with the total pressure of 1 kPa with a $TiCl_4$-$AlCl_3$-NH_3-H_2-He system using a hot-wall tubular reactor, whose diameter and length were 55 and 1150 mm, respectively. Planar cemented carbide (WC-Co) substrates or Si(100) substrates with micro-trenches were used. The growth rate was determined from the cross-sectional scanning electron microscope (SEM) images. The overall reaction rate constant k and the deposition species concentrations were calculated from the growth rate distribution on planar substrates in the reactor. On the other hand, surface reaction rate constant k_s and the number of deposition species were extracted from the relative film thickness distribution in a trench using the Microcavity method [3]. Chemical composition of the film was analyzed by X-ray photoelectron spectroscope (XPS). The calculation of the gas phase reaction was performed using simulation software ANSYS Chemkin-Pro.

3. Results and discussion

Figure 1(a) shows the dependence of the TiAlN growth rate on the $AlCl_3$ partial pressure with a constant $TiCl_4$ partial pressure. Decomposed growth rates of AlN and TiN components from a chemical composition of the TiAlN film. The AlN growth rate exhibits a first order reaction while the TiN growth rate decreases despite a constant supply of the Ti source. It suggests that TiAlN growth involves some interactive reactions among Ti and Al precursors. Figure 1(b) shows a similar trend to Fig. 1(a), which indicates the existence of interactive reactions. Therefore, the reaction mechanism of AlN and TiN was individually investigated in this study as a first step. Figure 2 shows the growth rate distribution of AlN and TiN along the reactor. The growth rate decreased exponentially along the flow direction, indicating that the film is deposited with the first order reaction. k was extracted from the slope of the figure, which was1.5 and 1.4 m/s for AlN and TiN, respectively. Next, we calculated the concentration of the deposition species at the respective position of the reactor. The deposition species of AlN and TiN at 60 mm were 1.7×10^{-4} and 1.6×10^{-4} mol/m^3, respectively. Figure 3 shows the relative film thickness distribution in the trench at several reactor positions. All of the film thickness distribution could be fitted well using the same k_s independent from the positions, which were 7 and 26 m/s for AlN and TiN, respectively. This suggests that only one deposition species contributes to film formation in both materials. Here, k_s was larger than k in the growth of both materials and k was close to the mass transfer coefficient k_d calculated from the reactor geometry and the Chapman-Enskog theory. Accordingly, both AlN and TiN were grown in the diffusion limited. Furthermore, the gas phase reaction was simulated using the previously reported gas phase reaction models to identify the deposition species [4-7]. Figure 4 shows the concentration of the gaseous species along the reactor. In both cases, metal sources were stable at this temperature and thus neither decomposed nor reacted with NH_3 sufficiently. Concentrations of $TiCl_4$ and $AlCl_3$ were both in the order of 10^{-4} mol/m^3 in the entire of the reactor, the values of which was identical to those extracted from Fig. 2. Therefore, the source materials are the deposition species in this system and the interactive reaction between Al and Ti precursors would occur not in the gas phase but on the growth surface.

Reference

[1] R. Zhang *et al*., Mater. Sci. Eng. A **448** (2007) 111. [2] I. Endler *et al*., Surf. Coat. Technol. **203** (2008) 5303. [3] L.S. Hong *et al*., Thin Solid Films **365** (2000) 176. [4] S. Umanskii *et al*., J. Comput. Chem. **22** (2001) 1366. [5] F. Teyssandier *et al.*, J. Electrochem. Soc. **145** (1998) 2167. [6] A. Dollet *et al.*, Thin Solid Films **406** (2002) 1. [7] M. Swiharta *et al.*, Combust. Flame **132** (2003) 91.

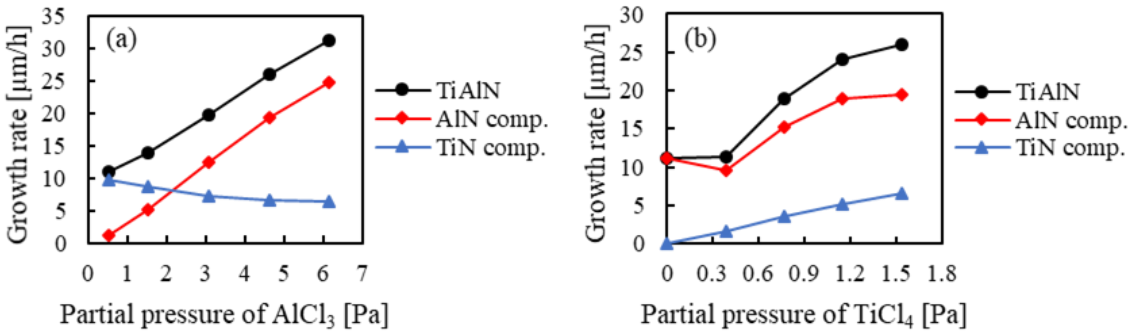

Figure 1. Dependence of growth rate on partial pressure of (a)$AlCl_3$ or (b)$TiCl_4$.

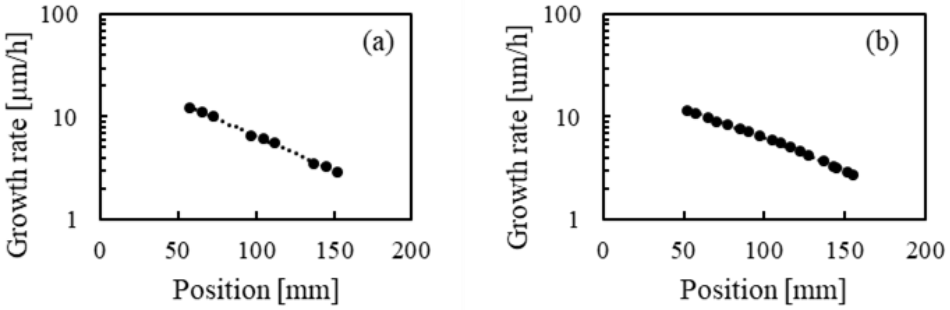

Figure 2. Distribution of growth rates of (a)AlN or (b)TiN in the reactor.

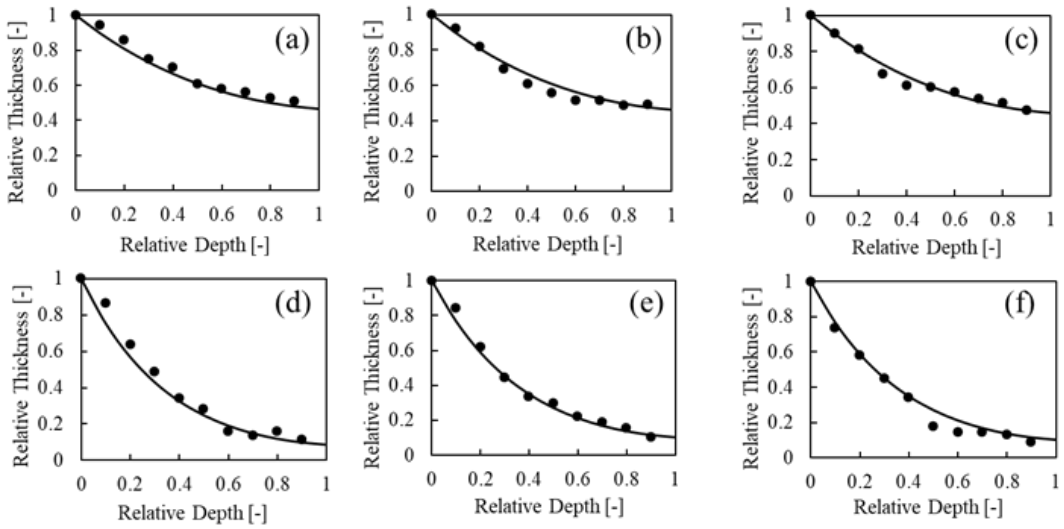

Figure 3. The relative film thickness distribution in the trench.
(a-c) AlN at the position of 60 mm, 100 mm, 140 mm, (d-f) TiN at 60 mm, 100 mm, 140 mm.

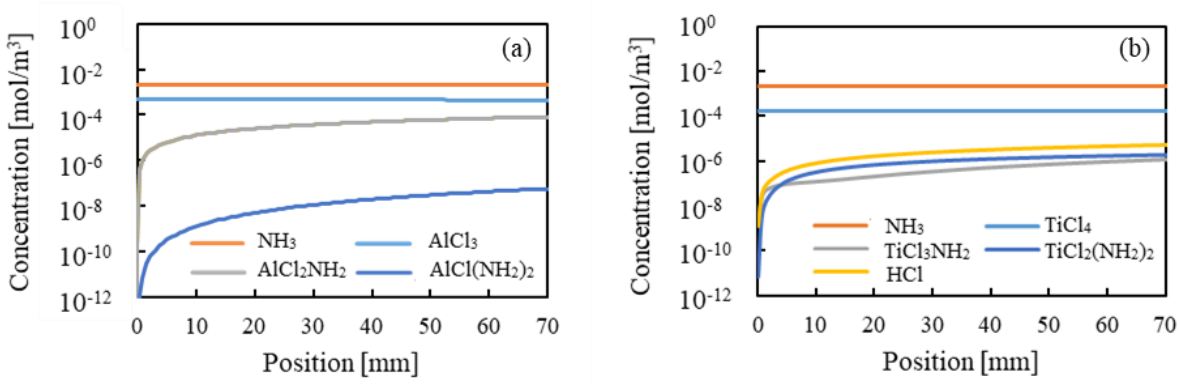

Figure 4. Calculated distribution of concentrations of precursors along the reactor in the gas phase.

Time-resolved in-situ mass spectrometry for monitoring and identifying reaction products in ALD processes

Andreas Werbrouck[1], Felix Mattelaer[1], Jolien Dendooven[1], Christophe Detavernier[1]

[1] Department of Solid State Sciences, COCOON group, Ghent University, Gent, Belgium (christophe.detavernier@ugent.be)

Several measurement techniques are available for *in-situ* monitoring of ALD processes. Microbalance, infrared spectroscopy and (spectroscopic) ellipsometry are well-established [1]. Compared to these techniques, the use of mass spectrometry is less common in the ALD field. Given the need for good time resolution, only a few masses can be studied simultaneously, often limiting the practical use of mass spectrometry to the detection of simple and small reaction products such as CH_4, CO and CO_2. For more complicated reaction chemistries, a time-resolved measurement of the full m/z-range is necessary, since this allows for fingerprinting reaction products by their entire mass-to-charge-spectrum instead of a single mass-to-charge ratio. A novel data acquisition method is described which allows for obtaining time-resolved, full mass-to-charge-range mass spectra to investigate ALD reaction chemistries. This method is demonstrated for the well-known TMA-H_2O ALD process for Al_2O_3 as a proof of concept, and its usefulness is further illustrated by its application to the LiHMDS-TMP process for the deposition of solid electrolyte Li_3PO_4 films reported by Hämäläinen *et al*. [2], as shown in figure 1.

The atomic layer deposition field proves an inherently difficult use case for mass spectrometry. In other fields where mass spectrometry is commonly employed (e.g. peptide synthesis), the source of molecules is quasi unlimited and there is only one species of interest to identify. In ALD process characterisation however, life is not that easy.
First of all, in an ALD process there is a background of precursor molecules/reactant gas with a known structure, which are of relatively little interest. The gaseous reaction products, which are of interest, are usually only present in small concentrations as they originate from the surface reactions in the reactor and are typically only present in the reaction chamber for a very limited time as they are continuously removed during the process. Measurements with good time resolution hence become paramount for a successful understanding of the reaction chemistry [3].
Secondly, it is impossible to distinguish the gaseous reaction products that originate from surface reactions on the reactor walls from those originating from the sample surface. This can be alleviated by increasing the signal-to-noise ratio (using a substrate with higher surface area) and considering proper background or baseline spectra.
Finally, since mass spectrometry relies on the ionizing and cracking of incoming molecules, the masses of detected fragments originating from the reaction products of interest are usually very similar to those of the originating precursor molecule. Spectral overlap compromises the assignment of a single m/z ratio to a molecule. This motivates the need for 'fingerprinting' complex by-products by their full spectrum.

Despite these hurdles, ALD processes have the advantage that they are of cyclic nature, so after the first cycles where initial growth effects could be of importance, the chemistry of each cycle should be identical and can be repeated as often as necessary to obtain data with good signal-to-noise ratio. In this work, we exploit this by combining data from several ALD cycles to construct a time-resolved m/z spectrum of the chemicals in one ALD cycle with a standard quadrupole mass spectrometer (Hiden HPR-30). This way, the aforementioned barriers can be surmounted, enabling complete mass spectrum analyses of ALD reaction chemistries.

[1] K. Knapas, M. Ritala. Author, CRIT REV SOLID STATE 38.3 (2013) 167-202
[2] J. Hämäläinnen, j. Holopainen, F. Munik, T. Hatanpää, M. Heikkilä, M. Ritala, M. Leskelä, J. Electrochem. Soc. 159.3 (2012) A259-A263
[3] I.J.M. Erkens, A.J.M. Mackus, H.C.M. Knoops, P. Smits, T.H.M. Van de Ven F. Roozeboom, W.M.M. Kessels, ECS J. Solid State Sci. Technol 1 (2012) P255-P262

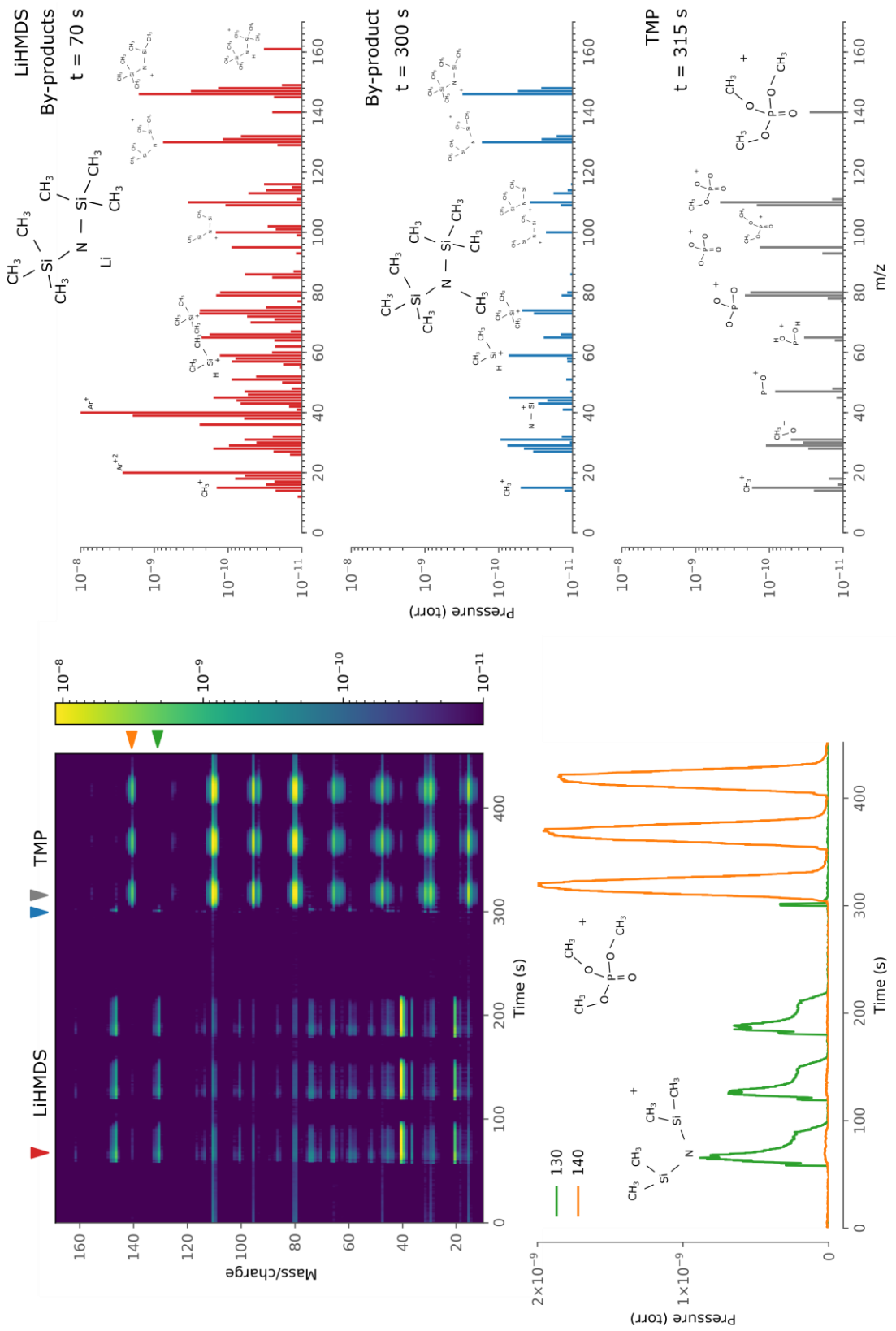

Figure 1. Illustration of the results obtained by the analysis method. Three pulses of lithium hexamethyl disilyl azide (LiHMDS) were followed by 3 pulses of trimethyl phosphate (TMP). This process results in a crystalline Li_3PO_4 film [2]. The heat map shows the full dataset, the other graphs are slices of a specific mass over charge ratio, similar to results obtained by a 'classical' measurement. The mass over charge spectra are taken at specific times indicated on the graphs. In this way the first pulse shows a sign of the reaction products, where the next pulses indicate the fingerprint of the precursor molecule. At t= 70 s, the LiHMDS peak is visible, together with groups from the TMP molecule that at that time are removed from the surface (red spectrum). A clear signature is visible at t=300, indicating that CH_3 from the TMP is taken by the $N(Si(CH_3)_3)_2$ ligand (blue spectrum). Finally the signature of the TMP precursor molecule (no reaction products) is observed at t = 315 s. Careful analysis of this kind of dataset can unravel the complex reaction mechanism.

Atomic layer deposition onto reinforcement fiber fabrics

Pauline Dill, Christian Militzer, Werner A. Goedel*

Chemnitz University of Technology, Physical Chemistry, 09111 Chemnitz, Germany

(pauline.dill@chemie.tu-chemnitz.de)

Carbon fiber fabrics with a size of 8 cm × 20 cm were coated via atomic layer deposition (ALD) with protective alumina coatings, using alternating pulses of timethyl aluminium and water. After 168 cycles a coating thickness of 30 ±6 nm could be determined via scanning electron microscopy (SEM) and thermogravimetric analysis (TGA) on nine parts of the fabric. Small pieces of coated fabric were cut out and subsequently oxidized under air at 700 °C. This oxidized the carbon and yields a fabric of interwoven alumina microtubes, which still resemble the shape of the original fabric. Micrographs of the fabric before and after oxidation are shown in Figure 1. The investigation of defects especially in the intersection points in the fabric was done by infiltrating the 'warp' and 'weft' tubes with two different fluorescent dye solutions and confocal fluorescence microscopy was performed. Even though the dye solution spill out of the microtubes at some points, it was concluded that the majority of initial coatings had a low defect density. [1]

Silicon carbide (SiC) fiber reinforced SiC ceramics are of very high interest as mechanically stable high-temperature materials. During the manufacturing process, the fiber fabrics are at first infiltrated by a carbon source and afterwards subjected to liquid silicon. But uncoated SiC fibers cannot even withstand the exposing to silicon vapor without being damage (Figure 2 e). A SEM image of the uncoated SiC fiber before is shown in Figure 2 a) and a Photo in Figure 2 c). In order to solve this problem SiC fiber fabrics were first coated with alumina via ALD (up to 0.5 µm/ 2600 cycles) and later embedded into the SiC matrix. At first experiments the coated SiC fiber fabrics were just exposed to silicon vapor at 1600 °C under vacuum. This resulted in a reaction of the coating with silicon vapor, but the fiber remained undamaged (Figur 2 f). SEM image of the coated SiC fiber before exposing to silicon vapor is shown in Figure 2 b. So there must be more

[1]Militzer C, Dill P, Goedel WA. Atomic layer deposition onto carbon fiber fabrics. *J Am Ceram Soc.* **2017**;100:5409-5420.

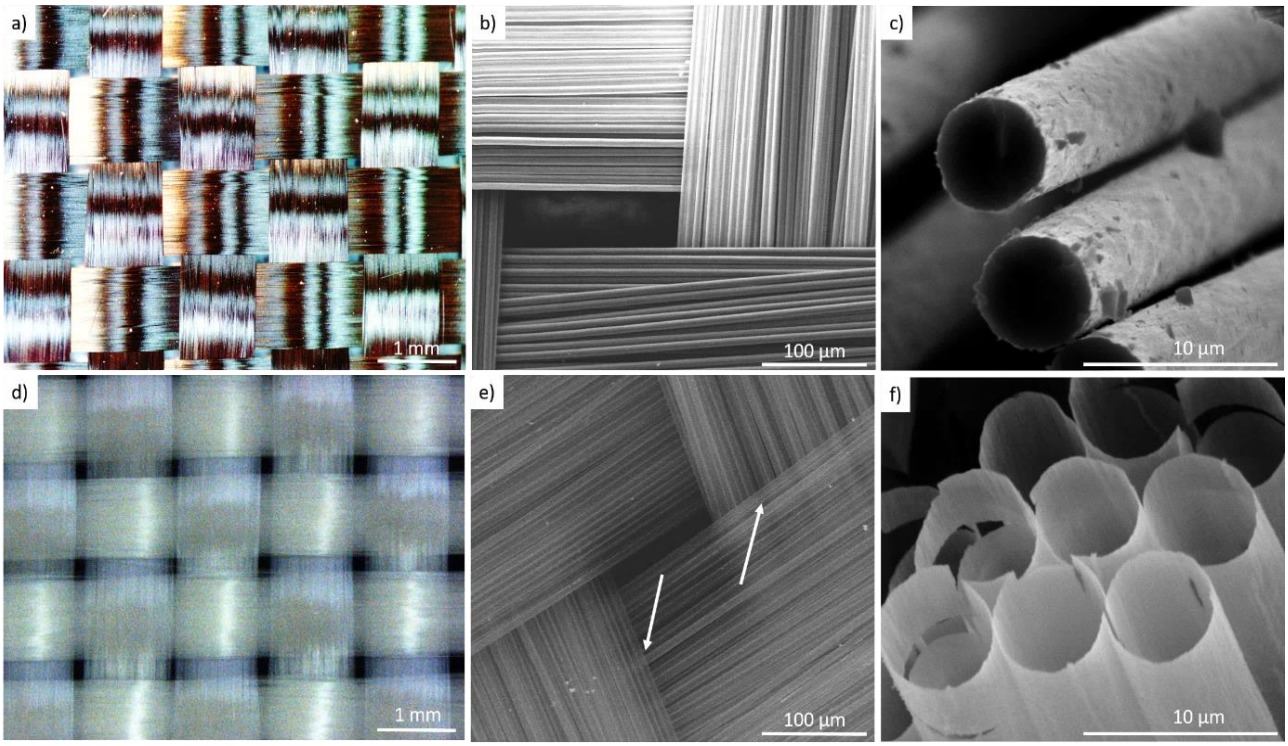

Figure 1. a,b,c) coated carbon fiber fabric; d,e,f) micro tubes after oxidation of the carbon fiber fabrics. A,d) light microscope; b,e) SEM image from top on the intersection; c,f) SEM image of the cross section of the fiber and the micro tubes.[1]

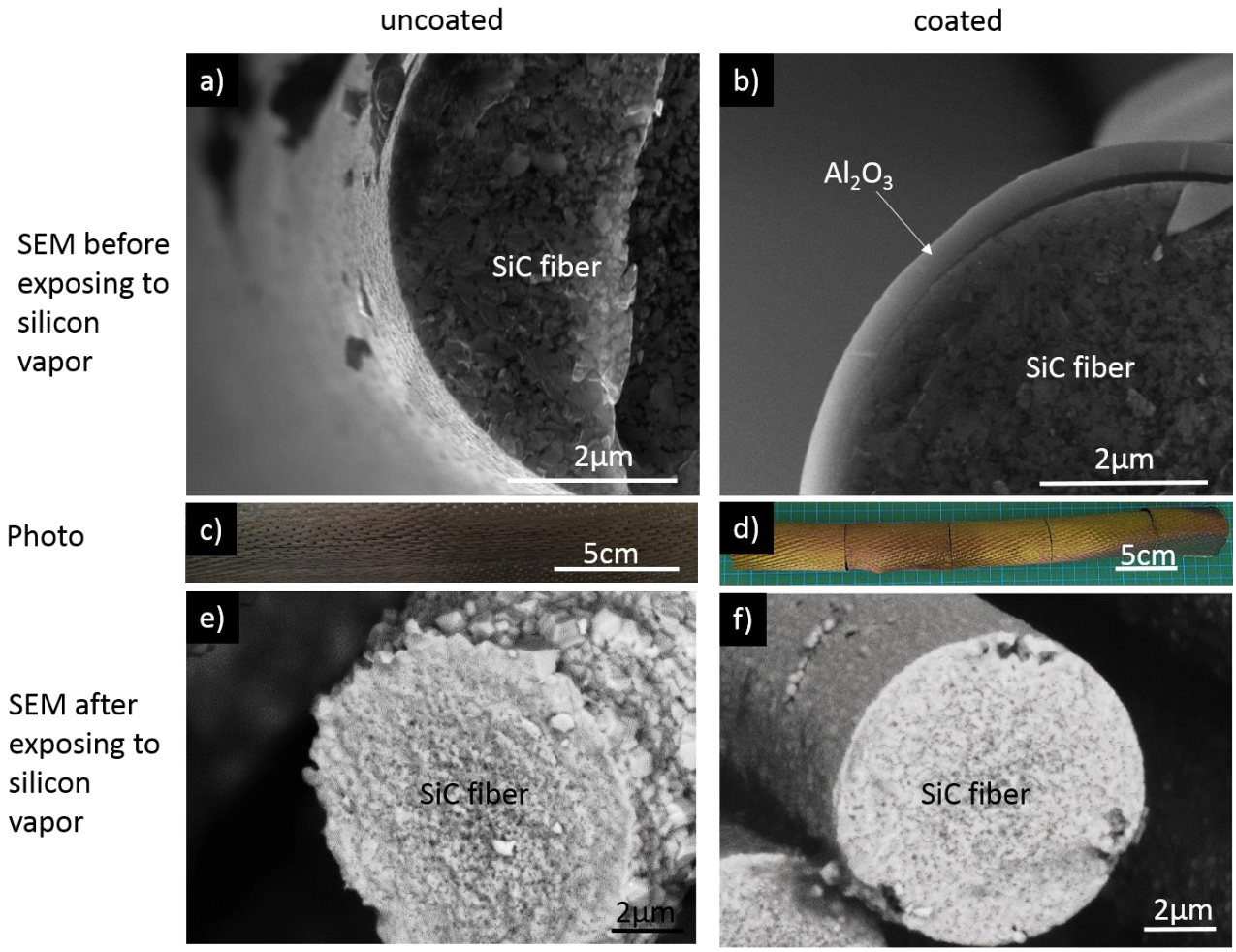

Figure 2. SEM image of the a) uncoated SiC fiber and the b) with alumina coated SiC fiber. And c) photo of the uncoated SiC fiber fabric and d) photo of the coated SiC fiber fabric. After the coating, the color of the surface changed from black to green. SEM image after exposing the SiC fiber fabrics to silicon vapor e) without coating and f) with coating.

Experimental and numerical study of an oCVD process for the deposition of PEDOT thin films

M. Mirabedin*[1], A. Pezzoli[1, 2], H. Vergnes[1], C. Vahlas[2], N. Causse[2], B. Caussat[1]

1 Laboratoire de Génie Chimique, Université de Toulouse, CNRS, INPT, UPS, Toulouse, France.

2 CIRIMAT, Université de Toulouse, CNRS, INPT, UPS, Toulouse, France.

brigitte.caussat@ensiacet.fr

The research area of organic electronics has grown dramatically since the discovery of the first conductive polymer in 1977, due to numerous promising applications under development [1]. One of the most efficient conducting polymers is poly 3, 4ethylenedioxythiophene (PEDOT). Deposition techniques of PEDOT, are limited by the rigid nature of the conjugated backbone inducing quasi-insolubility. Spin-coating of PEDOT doped with polystyrene sulfonic acid (PSS) emulsion (PEDOT:PSS) leads to inherently low conductivities of ca. 10 S/cm. High conductivity (300 S/cm) PEDOT thin films have been synthesized by electropolymerization [2], but a conductive substrate is required in this case. All these techniques present issues of solvent-substrate compatibility and film contamination by the solvent as they are prepared in liquid phase. Oxidative polymerization can also yield PEDOT thin films but the process reproducibility is poor and operating parameters are limited [3]. Alternatively, oxidative chemical vapor deposition (oCVD) of PEDOT films is a simple one-step gas phase process, which enables the formation of conformal films of conducting polymers at low temperature on complex surface structures [4]. oCVD is particularly promising for thermal or solvent sensible substrates and complex geometries [5] (for example: paper, fabrics or polymeric membranes). The oCVD process conditions, such as substrate temperature, absolute pressure and flow rates, can be varied in order to get insight in the process and the polymer structure and to adjust the electrical properties required for successful integration in organic devices.

In this presentation, we report on the experimental and reactor scale simulation results of an oCVD process for the deposition of PEDOT films. The oCVD reactor allows deposition on a variety of substrates such as ϕ10 cm Si wafers, complex 3D objects, tissue or paper, and is schematically presented in Figure 1(a). Numerical simulations of gas flow and thermal profile inside the reactor are obtained using ANSYS Fluent v18.2, as illustrated in Figure 1(b) showing the velocity profile of the gas phase in one processing conditions. A quartz crystal microbalance is implemented in the reactor; it provides deposition rate data in terms of frequency such as the one shown in Figure 2. These are used to develop apparent kinetic laws of PEDOT deposition, in order to establish the correlations between deposition conditions and local film thickness and composition.

Running investigations concern the interplay between the oxidant ($FeCl_3$), carrier gas (N_2) and monomer (EDOT) flow rates, the substrate temperature and the process pressure in on hand, with the film deposition rate, morphology, chemical composition and electrical conductivity on the other. Preliminary results show that 40 to 800 nm thick films processed at 13 Pa at ambient temperature are composed of PEDOT as shown in the FTIR spectrum of Figure 3. Their conductivity strongly depends on the oxidant and monomer flow rates [6]. Conductivities between 0.1 and 300 S/cm are measured.

[1] Forrest, S.R., Nature, 2004. **428**(6986): p. 911.
[2] Yamato, H., et al., Synthetic metals, 1996. **83**(2): p. 125-130.
[3] Winther-Jensen, B., D.W. Breiby, and K. West, Synthetic metals, 2005. **152**(1-3): p. 1-4.
[4] Tenhaeff, W.E. and K.K. Gleason, Advanced Functional Materials, 2008. **18**(7): p. 979-992.
[5] Lock, J.P., 2005, Massachusetts Institute of Technology.
[6] Im, S.G., 2009, Massachusetts Institute of Technology.

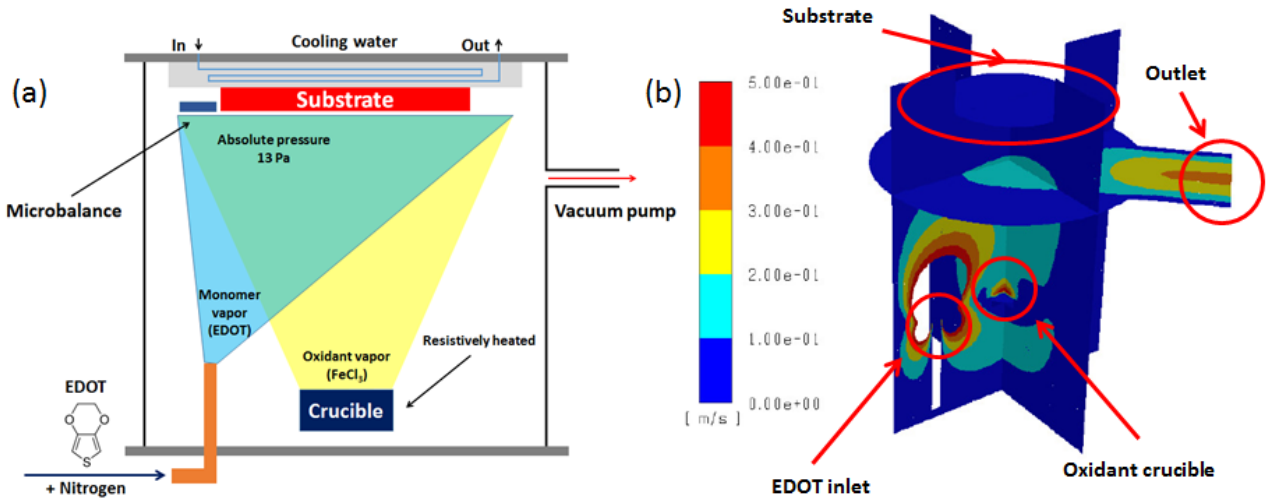

Figure 1. (a): Schematic of oCVD reactor ,(b): gas velocity profile inside the reactor (velocity zones higher than 0.5 m/s are not presented)

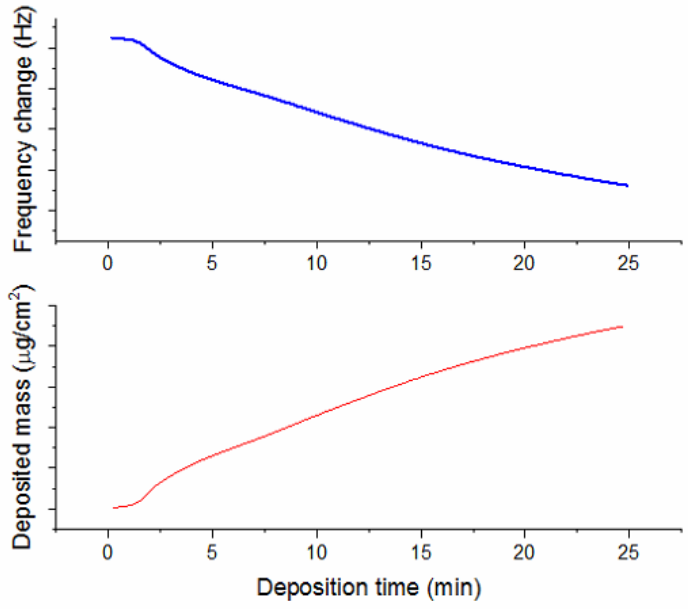

Figure 2. Microbalance mass gain along deposition time as shown by frequency reduction

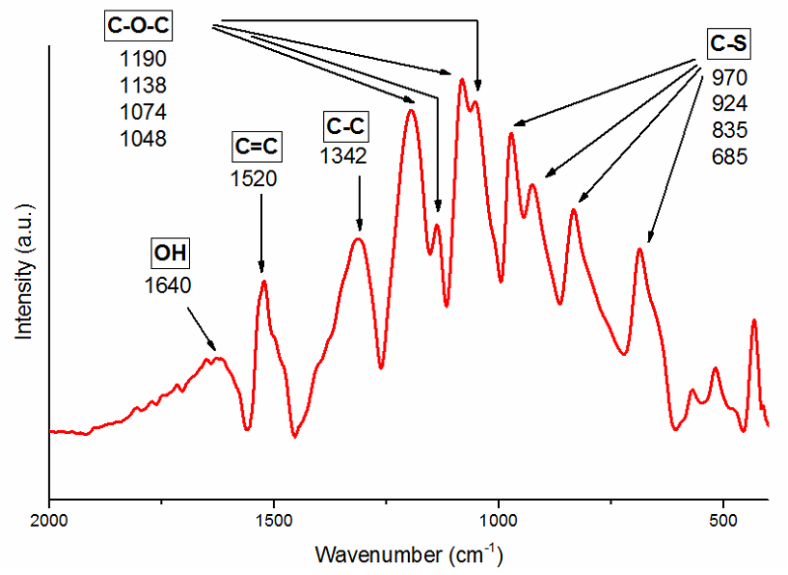

Figure 3. Typical FTIR spectrometry data of a PEDOT sample

From precursor design to growth mechanisms - ab initio modelling of CVD processes for III/V materials

Ralf Tonner

Department of Chemistry, Philipps-Universität Marburg, Hans-Meerwein-Straße 4, Marburg, Germany (tonner@chemie.uni-marburg.de)

Progress in thin-film deposition methods often depends on our understanding of the underlying elementary steps at the level of atomic and electronic structure. For key questions, theoretical investigations can help by complementing the experimental investigations. Nevertheless, the goal for theoretical approaches is to move beyond interpretation of already available data and provide predictions and guidance for future investigations. Predictive computations require high accuracy which directly leads to ab initio methods like density functional theory (DFT) or wave function-based methods combined with methods for larger length and time scales like kinetic Monte Carlo (kMC).

The low-temperature growth of GaP on H/Si(001) by metal-organic vapor phase epitaxy (MOVPE) is taken as an example to highlight the strengths (and limitations) of these ab initio approaches (Figure 1). For the first step - the gas phase decomposition of precursors - we find very high barriers for several reactions proposed earlier for *tert*-butylphosphine (TBP) and triethylgallane (TEGa) and unusual β-H elimination reactions relevant for ligand design.[1] DFT approaches including methods for treating dispersion interactions (DFT-D) are in good agreement with gold-standard quantum chemical coupled-cluster methods.

This lends confidence for using these methods to reveal characteristics of surface adsorption for TBP – accurate enough to predict the outcome of growth experiments and ex-situ scanning tunneling microscopy measurements. Unusual electronic vacancy stabilization effects are revealed by theory to lead to non-statistical growth in the nucleation phase.[2]

In a joint endeavor of experiment and theory, we could further reveal the thermodynamic and kinetic reasons for the unexpected structure of GaP/Si interfaces. Intermixing models established previously are not sufficient to explain the pyramidal structure observed experimentally. Instead, relative facet stabilities and ad-atom mobility in the interface region needs to be quantified to find a rationale for the atomically-resolved measurements.[3]

Further fruitful experiment-theory collaborations resulted in transfer of these ideas and approaches toward modelling of chemical vapor deposition (CVD) of boron carbides and other compound semiconductors.[4]

Despite what has been achieved up to know, significant challenges for the theoretical modelling of such complex experimental procedures remain and will be outlined.

[1] a) A. Stegmüller, P. Rosenow, R. Tonner, PCCP, 16 (2014) 17018; b) A. Stegmüller, R. Tonner, Inorg. Chem. 54 (2015) 6363; c) A. Stegmüller, R. Tonner, Chem. Vap. Deposition 21 (2015) 161.

[2] A. Stegmüller, K. Werner, M. Reutzel, A. Beyer, P. Rosenow, U. Höfer, W. Stolz, K. Volz, M. Dürr, R. Tonner, Chem.--Eur. J. 22 (2016) 14920.

[3] A. Beyer, A. Stegmüller, J. O. Oelerich, K. Jandieri, K. Werner, G. Mette, W. Stolz, S. D. Baranovskii, R. Tonner, K. Volz, Chem. Mater. 28 (2016) 3265.

[4] a) M. Imam, K. Gaul, A. Stegmüller, C. Hoglund, J. Jensen, L. Hultman, J. Birch, R. Tonner, H. Pedersen, J. Mat. Chem. C 3 (2015) 10898; b) M. Imam, L. Souqui, J. Herritsch, A. Stegmüller, C. Hoglund, S. Schmidt, R. Hall-Wilton, H. Hogberg, J. Birch, R. Tonner, H. Pedersen, J. Phys. Chem. C 121 (2017) 26465; c) E. Sterzer, A. Beyer, L. Durschek, B. Ringler, B. T. Leube, A. Stegmüller, R. Tonner, C. von Hänisch, W. Stolz, K. Volz, J. Cryst. Growth 439 (2016) 19.

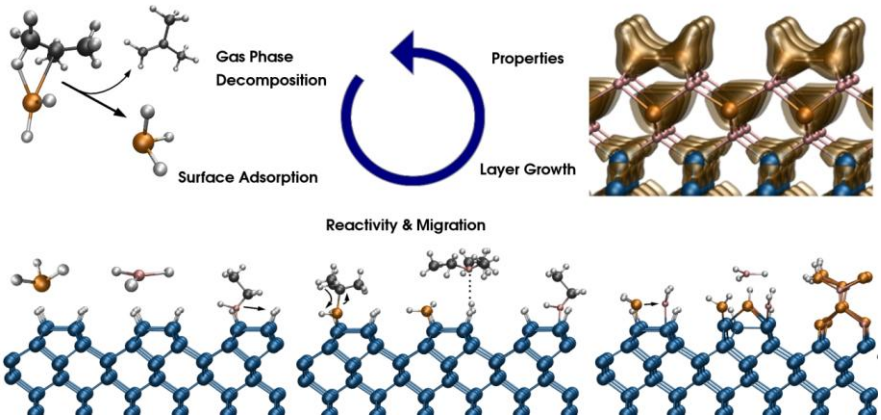

Figure 1. Elemental steps for modelling in metal-organic vapor phase epitaxy.

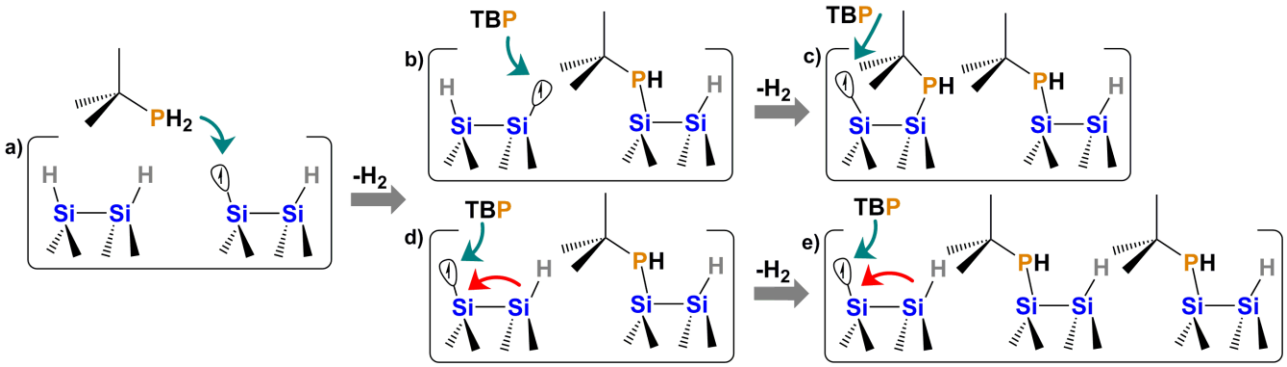

Figure 2. Growth model for TBP on H/Si(001) derived from theory and experiment.